Journal of Engineering Mathematics **44:** 207–228, 2002.

Flame quenching through endothermic reaction

A. LAZAROVICI[1], S. KALLIADASIS[2], J.H. MERKIN[1] and S.K. SCOTT[3]
[1]*Department of Applied Mathematics*
[2]*Department of Chemical Engineering*
[3]*School of Chemistry, University of Leeds, Leeds, LS2 9JT UK*

Received 10 August 2001; accepted in revised form 6 June 2002

Abstract. A laminar premixed flame model is considered in which there is a second-order branching reaction coupled with an endothermic decay of a chemical inhibitor. An analysis, based on high activation energies for the reactions, is performed and two distinct cases are found. These depend on dimensionless parameters representing the loss of heat relative to its production, α, and the consumption of inhibitor relative to that of fuel, β. With $\alpha \sim \beta \ll 1$, extinction is achieved through a saddle-node bifurcation at a critical value of α. For $\alpha \ll \beta$, no extinction is found though considerable reductions in wave speed over the adiabatic limit are seen. The asymptotic results are compared with numerical simulations of an initial-value problem for the model.

Key words: combustion, endothermic inhibition, high-activation-energy asymptotics, propagating flames

1. Introduction

Premixed flames have been extensively studied as they are central to many technological processes; extensive reviews are provided by Buckmaster and Ludford [1], Williams [2] and Zeldovich *et al.* [3]. An important feature in any consideration of premixed flames is propagation inhibition (or flame quenching). The original discussions on this aspect were concerned with situations where the removal of the heat created in the combustion reaction was through purely temperature-dependent cooling (usually modelled by Newtonian cooling — a linear temperature dependence). In these cases flame quenching is abrupt, occurring at a saddle-node bifurcation at some critical value of the appropriate heat loss parameter. This was clearly demonstrated through the use of high activation energy asymptotics in the definitive paper by Buckmaster [4]. More recently these ideas have been extended to two-dimensional bifurcations [5] and to a two-step branching-recombination reaction with a volumetric heat loss [6].

An alternative route by which the heat generated in the exothermic combustion reaction can be dissipated is by some additional endothermic reaction. To examine this process in more detail we consider a prototype model. In our model we assume that there are two active chemical species, a fuel A, which undergoes a second-order exothermic reaction

$$A + A \to B \qquad \text{rate: } R_A = k_1 a^2 \mathrm{e}^{-E_1/RT}, \quad Q_1 > 0 \tag{1}$$

and a chemical inhibitor W, which decays to an inert product through the endothermic reaction

$$W \to P \qquad \text{rate: } R_W = k_2 \overline{w} \mathrm{e}^{-E_2/RT}, \quad Q_2 < 0. \tag{2}$$

Here a and $\overline{w}$ are the concentrations of reactants A and W, T is (absolute) temperature, $k_1,\ k_2$ are the pre-exponential factors and $E_1,\ E_2$ are the activation energies in reactions (1) and (2),

respectively, R is the universal gas constant. A motivation for our model is provided by our previous discussion of the effects of endothermic reactions coupled with radical scavenging on branched-chain flame reactions [7]. Chemical reactions (1) and (2) played an important role in this study, the second-order step (1) arose in [7] from an initiation and branched-chain reaction being in quasi-steady state.

The significant feature that arises in our analysis is that both front and pulse waves in the temperature are possible (fronts show a rise in temperature through the wave from the initial 'cold' state; in a pulse the temperature returns to its original state). When there is purely temperature-dependent cooling, only pulse waves are possible. Which type of waveform arises in our model depends effectively on the relative values of two (dimensionless) parameters α and β that we indentify below. α measures the heat loss through the endothermic reaction (2) against its generation via step (1), β gives the rate of consumption of the inhibitor W relative to that of the fuel A. These two parameters are also the important ones in determining whether there is wave inhibition or not. Flame quenching, when it occurs, is through the usual saddle-node bifurcation and, even when it does not occur, there are considerable reductions in propagation speed as the effects of the cooling become more pronounced.

We start by deriving the equations governing our model. These are made dimensionless, following the previous paper by Buckmaster [4], so as to make them suitable for high activation asymptotics, which is the main part of our paper. These asymptotic results are augmented by numerical simulations of the model.

2. Model

To derive the heat and mass balance equations for our model we assume a thermal/diffusive model. This model is valid in the limit of weak thermal expansion, when there is no coupling of the temperature and reactant concentrations with the underlying flow field. This approach has been used extensively in the past, see the recent work of Weber *et al.* [8] and Mercer *et al.* [9]. This leads to the equations for our model as

$$\begin{aligned} \rho C_p \frac{\partial T}{\partial t} &= \kappa \frac{\partial^2 T}{\partial x^2} + Q_1 k_1 a^2 \mathrm{e}^{-E_1/RT} - Q_2 k_2 \overline{w} \mathrm{e}^{-E_2/RT}, \\ \frac{\partial a}{\partial t} &= D_A \frac{\partial^2 a}{\partial x^2} - k_1 a^2 \mathrm{e}^{-E_1/RT}, \\ \frac{\partial \overline{w}}{\partial t} &= D_W \frac{\partial^2 \overline{w}}{\partial x^2} - k_2 \overline{w} \mathrm{e}^{-E_2/RT} \end{aligned} \tag{3}$$

where D_A, D_W are the diffusion coefficients for species A and W, κ is the thermal conductivity (all assumed constant) and C_p is the specific heat at constant pressure.

Initially the fuel and inhibitor are uniformly distributed with concentrations a_0 and w_0, respectively. For simplicity, we make the further assumption that initially $T = 0$ everywhere except in some (small) region centred on $x = 0$. In this region there is a temperature input to initiate the reaction and allow the possible formation of travelling combustion waves.

To make Equations (3) dimensionless we adopt the scalings suggested by Buckmaster [4], as this leads to a system that is readily amenable to the high-activation-energy asymptotics that we wish to consider. We put

$$T = \left(\frac{Q_1 a_0}{\rho C_p}\right) u,\ v\ =\ \frac{(a_0 - a)}{a_0},\ w = \frac{(w_0 - \overline{w})}{w_0},$$
$$\overline{t}\ =\ \left(k_1 a_0 \mathrm{e}^{-\gamma}\right) t,\ \overline{x} = \left(\frac{\rho C_p k_1 a_0 \mathrm{e}^{-\gamma}}{\kappa}\right)^{1/2} x, \tag{4}$$

where γ, the dimensionless activation energy parameter, is given by

$$\gamma = \frac{\rho C_p E_1}{R Q_1 a_0}. \tag{5}$$

Substitution of (4, 5) in Equations (3) leads to the dimensionless equations for our model as (on dropping the bars for convenience)

$$\frac{\partial u}{\partial t} = \frac{\partial^2 u}{\partial x^2} + (1-v)^2 \exp\left(\frac{\gamma(u-1)}{u}\right) - \alpha(1-w)\exp\left(\frac{\mu\gamma(u-1)}{u}\right), \tag{6}$$

$$\frac{\partial v}{\partial t} = \frac{1}{L_A}\frac{\partial^2 v}{\partial x^2} + (1-v)^2 \exp\left(\frac{\gamma(u-1)}{u}\right), \tag{7}$$

$$\frac{\partial w}{\partial t} = \frac{1}{L_W}\frac{\partial^2 w}{\partial x^2} + \beta(1-w)\exp\left(\frac{\mu\gamma(u-1)}{u}\right), \tag{8}$$

where

$$\mu = \frac{E_2}{E_1}, \quad \alpha = \frac{Q_2 k_2 w_0 \mathrm{e}^{\gamma(1-\mu)}}{Q_1 k_1 a_0^2}, \quad \beta = \frac{k_2 \mathrm{e}^{\gamma(1-\mu)}}{k_1 a_0}$$

are dimensionless reaction parameters and

$$L_A = \frac{\kappa}{D_A \rho C_p}, \quad L_W = \frac{\kappa}{D_W \rho C_p}$$

are the Lewis numbers associated with the fuel and inhibitor, respectively. Note that

$$\frac{\alpha}{\beta} = \frac{Q_2 w_0}{Q_1 a_0}.$$

The initial conditions are that

$$u = u_0 g(x), \quad v = w = 0 \quad \text{at } t = 0\ (-\infty < x < \infty), \tag{9}$$

where $g(x)$ is a smooth function with compact support. For the numerical simulations described below we apply zero-flux boundary conditions at infinity and, for simplicity, assume symmetry about $x = 0$, taking

$$\frac{\partial u}{\partial x} = \frac{\partial v}{\partial x} = \frac{\partial w}{\partial x} = 0 \quad \text{at } x = 0 \quad \text{and as } x \to \infty\ (t > 0). \tag{10}$$

2.1. Travelling-wave equations

Our main purpose is to investigate the possible initiation (and properties) of any steady propagating combustion waves that our model (6–10) can support. The equations governing such waves are obtained by introducing the travelling co-ordinate

$$y = x - ct,$$

where c is the (constant) wave speed, which we can take as positive, and then looking for solutions in terms of the single co-ordinate y. This leads to the travelling-wave equations

$$u'' + cu' + (1-v)^2 \mathrm{e}^{\dfrac{\gamma(u-1)}{u}} - \alpha(1-w)\mathrm{e}^{\dfrac{\mu\gamma(u-1)}{u}} = 0, \tag{11}$$

$$\frac{1}{L_A}v'' + cv' + (1-v)^2 \mathrm{e}^{\dfrac{\gamma(u-1)}{u}} = 0, \tag{12}$$

$$\frac{1}{L_W}w'' + cw' + \beta(1-w)\mathrm{e}^{\dfrac{\mu\gamma(u-1)}{u}} = 0, \tag{13}$$

subject to

$$u \to 0, \quad v \to 0, \quad w \to 0 \quad \text{as } y \to \infty, \tag{14}$$

(primes denote differentiation with respect to y).

At the rear of the wave, conditions have to be uniform with the reaction completed. Equations (11–13) give the two possibilities:

$$u \to 0, \quad \text{and} \quad v \to v_s,\ w \to w_s \quad \text{as } y \to -\infty. \tag{15}$$

We shall refer to this case a *pulse wave* (in the temperature) or

$$v \to 1,\ w \to 1,\ u \to u_s \quad \text{as } y \to -\infty. \tag{16}$$

This is a *front wave* (all the fuel and inhibitor used up in the reaction). Here u_s, v_s and w_s are positive constants (to be determined).

If we combine Equations (11–13) to eliminate the reaction terms, integrate once and apply boundary conditions (14) as $y \to \infty$, we obtain

$$u' + cu - \left(\frac{1}{L_A}v' + cv\right) + \frac{\alpha}{\beta}\left(\frac{1}{L_W}w' + cw\right) = 0. \tag{17}$$

Hence for

$$\begin{aligned} &\text{Front waves:} \quad u_s = 1 - \frac{\alpha}{\beta} \\ &\text{Pulse waves:} \quad \beta v_s = \alpha w_s \end{aligned} \tag{18}$$

From (18) a necessary condition for the existence of a front wave is that $\alpha < \beta$ or $Q_1 a_0 > Q_2 w_0$.

3. High-activation-energy asymptotics, $\gamma \gg 1$

Here we develop a solution of the travelling-wave equations (11–13) valid for γ large. We adopt the approach developed by Buckmaster [4] for systems where the heat loss is through purely temperature-dependent (Newtonian) cooling. Here the heat loss is through the endothermic decay of the inhibitor. Our asymptotic approach requires that the parameters α, β and the wave speed c are all small. In particular, we require that

$$c = \overline{c}\,\gamma^{-3/2} \tag{19}$$

for a consistent matching in our asymptotic analysis, where $\overline{c}$ is $O(1)$ for γ large. We assume that $L_A,\ L_W$ are of $O(1)$.

We consider two separate cases, $\alpha \sim \beta$ and $\alpha \ll \beta$. In the first case we require $\alpha \sim \beta \sim \gamma^{-4}$ and that $\mu\gamma$ is of $O(1)$ to develop the appropriate asymptotic solution. We start with this case.

3.1. $\alpha \sim \beta \sim \gamma^{-4}$

Here we put

$$\alpha = \overline{\alpha}\,\gamma^{-4}, \qquad \beta = \overline{\beta}\,\gamma^{-4}, \qquad \nu = \mu\gamma, \tag{20}$$

where $\overline{\alpha}$, $\overline{\beta}$ and ν are of $O(1)$ as $\gamma \to \infty$. We start the solution in the region ahead of the reaction (Region I, the preheat zone). In this region we leave u and v unscaled and put

$$\overline{y} = y\gamma^{-3/2}, \quad w = \overline{w}\gamma^{-1}. \tag{21}$$

Expressions (19–21) are substituted in Equations (11–13) and a solution of the resulting equations is sought by expanding

$$u = u_0 + \gamma^{-1}u_1 + \cdots,\ v = v_0 + \gamma^{-1}v_1 + \cdots,\ \overline{w} = w_0 + \gamma^{-1}w_1 + \cdots$$
$$\overline{c} = c_0 + \gamma^{-1}c_1 + \cdots,$$

We find, consistent with matching with the reaction zone, that

$$\begin{aligned}
u_0 &= \mathrm{e}^{-c_0\overline{y}},\\
u_1 &= (T_1 - c_1\overline{y})\mathrm{e}^{-c_0\overline{y}} + \frac{\overline{\alpha}}{\nu c_0}\int_{\overline{y}}^{\infty} \mathrm{e}^{-c_0 s}\exp[\nu(1-\mathrm{e}^{c_0 s})]\mathrm{d}s,\\
v_0 &= \mathrm{e}^{-L_A c_0\overline{y}},\\
v_1 &= -L_A c_1\overline{y}\mathrm{e}^{-L_A c_0\overline{y}},\\
w_0 &= \frac{\overline{\beta}}{c_0}\left[\int_{\overline{y}}^{\infty}\exp\left(\nu(1-\mathrm{e}^{c_0 s})\right)\mathrm{d}s - \mathrm{e}^{-L_W c_0\overline{y}}\int_{\overline{y}}^{\infty}\mathrm{e}^{L_W c_0 s}\exp\left(\nu(1-\mathrm{e}^{c_0 s})\right)\mathrm{d}s\right] + B_0\mathrm{e}^{-L_W c_0\overline{y}}
\end{aligned} \tag{22}$$

(T_1 and B_0 are constants to be determined). To complete the matching with the reaction zone, we need the form of the solution in Region I for $\overline{y}$ small.

$$\begin{aligned}
u &\sim 1 - c_0\overline{y} + \frac{c_0^2\overline{y}^2}{2} + \cdots + \gamma^{-1}\left((T_1 + \frac{\overline{\alpha}I_\nu}{\nu c_0^2}) - (c_0T_1 + c_1 + \frac{\overline{\alpha}}{\nu c_0})\overline{y} + \cdots\right) + \cdots,\\
v &\sim 1 - L_A c_0\overline{y} + \frac{L_A^2 c_0^2\overline{y}^2}{2} + \cdots + \gamma^{-1}(-L_A c_1\overline{y} + \cdots) + \cdots,\\
w &\sim \gamma^{-1}\left(\frac{\overline{\beta}}{c_0^2}(J_\nu - K_\nu) + B_0 + \left(\frac{\overline{\beta}}{c_0^2}K_\nu - B_0\right)L_W c_0\overline{y} + \cdots\right),
\end{aligned} \tag{23}$$

where I_ν, J_ν and K_ν are the integrals

$$I_\nu = c_0 \int_0^\infty \mathrm{e}^{-c_0 y} \exp[\nu(1-\mathrm{e}^{c_0 y})]\mathrm{d}y = \int_0^\infty \frac{\mathrm{e}^{-\nu s}}{(1+s)^2}\mathrm{d}s = 1 - \nu \mathrm{e}^{\nu}\mathrm{ei}(\nu),$$

$$J_\nu = c_0 \int_0^\infty \exp[\nu(1-\mathrm{e}^{c_0 y})]\mathrm{d}y = \mathrm{e}^{\nu}\mathrm{ei}(\nu) = I_\nu - I_\nu',$$

$$K_\nu = c_0 \int_0^\infty \mathrm{e}^{L_W c_0 y} \exp[\nu(1-\mathrm{e}^{c_0 y})]\mathrm{d}y = \nu^{-L_W}\mathrm{e}^{\nu} \int_\nu^\infty s^{L_W - 1}\mathrm{e}^{-s}\mathrm{d}s,$$

where $\mathrm{ei}(\nu)$ is the exponential integral [10, p.470]. Note that $I_\nu \to 1$ as $\nu \to 0$, is monotone decreasing in ν, with $I_\nu \sim \nu^{-1}$ as $\nu \to \infty$.

We next consider the reaction zone (Region II), in which we put

$$u = 1 - \frac{U}{\gamma}, \quad v = 1 - \frac{V}{\gamma}, \quad w = \frac{W}{\gamma}, \quad \zeta = \gamma^{-1/2} y = \overline{y}\gamma. \tag{24}$$

Substituting (24) in Equations (11–13) gives

$$U'' - V^2 \exp\left(-\frac{U}{(1-\gamma^{-1}U)}\right) + \gamma^{-1}\overline{c}U' + \gamma^{-2}\overline{\alpha}(1-\frac{W}{\gamma})\exp\left(-\frac{\nu U}{\gamma(1-\gamma^{-1}U)}\right) = 0, \tag{25}$$

$$\frac{1}{L_A}V'' - V^2 \exp\left(-\frac{U}{(1-\gamma^{-1}U)}\right) + \gamma^{-1}\overline{c}V' = 0, \tag{26}$$

$$\frac{1}{L_W}W'' + \gamma^{-1}\overline{c}W' + \gamma^{-2}\overline{\beta}(1-\frac{W}{\gamma})\exp\left(-\frac{\nu U}{\gamma(1-\gamma^{-1}U)}\right) = 0, \tag{27}$$

where primes denote differentiation with respect to ζ.

We look for a solution of Equations (25–27) by expanding

$$U = U_0 + \gamma^{-1}U_1 + \cdots, \; V = V_0 + \gamma^{-1}V_1 + \cdots, \; W = W_0 + \gamma^{-1}W_1 + \cdots.$$

At leading order we obtain

$$U_0'' - V_0^2\mathrm{e}^{-U_0} = 0, \quad \frac{1}{L_A}V_0'' - V_0^2\mathrm{e}^{-U_0} = 0, \qquad W_0'' = 0, \tag{28}$$

subject to the matching condition, obtained by expressing (23) in terms of ζ and using (24),

$$U_0 \sim c_0\zeta - \left(T_1 + \frac{\overline{\alpha}I_\nu}{\nu c_0^2}\right), \quad V_0 \sim L_A c_0 \zeta, \quad W_0 \to \frac{\overline{\beta}}{c_0^2}(J_\nu - K_\nu) + B_0 \quad \text{as } \zeta \to \infty. \tag{29}$$

Eliminating the reaction terms in Equations (28), integrating and applying the matching conditions (29) as $\zeta \to \infty$, we have

$$U_0 = \frac{1}{L_A}V_0 - \left(T_1 + \frac{\overline{\alpha}I_\nu}{\nu c_0^2}\right), \qquad W_0 = \frac{\overline{\beta}}{c_0^2}(J_\nu - K_\nu) + B_0. \tag{30}$$

Substituting the first of these expressions in Equation (28a), integrating and satisfying the condition that $U_0' \to c_0$ as $U_0 \to \infty$ (as $\zeta \to \infty$) we obtain

$$U_0'^2 = c_0^2 - 2L_A^2 \mathrm{e}^{-U_0}\left(\left(U_0 + T_1 + \frac{\overline{\alpha} I_\nu}{\nu c_0^2}\right)^2 + 2\left(U_0 + T_1 + \frac{\overline{\alpha} I_\nu}{\nu c_0^2}\right) + 2\right). \tag{31}$$

At the rear of the reaction zone (Region II) $V_0 \to 0$ and hence

$$U_0 \to -\left(T_1 + \frac{\overline{\alpha} I_\nu}{\nu c_0^2}\right) \quad \text{as } \zeta \to -\infty.$$

Then, from (31),

$$c_0^2 = 4L_A^2 \exp\left(T_1 + \frac{\overline{\alpha} I_\nu}{\nu c_0^2}\right). \tag{32}$$

At $O(\gamma^{-1})$ we obtain the equations

$$\begin{aligned} U_1'' + c_0 U_0' - \mathrm{e}^{-U_0}\left(2V_1V_0 - V_0^2(U_1 + U_0^2)\right) &= 0, \\ \frac{1}{L_A}V_1'' + c_0 V_0' - \mathrm{e}^{-U_0}\left(2V_1V_0 - V_0^2(U_1 + U_0^2)\right) &= 0, \\ \frac{1}{L_W}W_1'' + c_0 W_0' &= 0, \end{aligned} \tag{33}$$

subject to the matching conditions, from (23), that

$$\begin{aligned} U_1 &\sim -\frac{c_0^2\zeta^2}{2} + \left(c_0 T_1 + c_1 + \frac{\overline{\alpha}}{\nu c_0}\right)\zeta + T_2 + \cdots, \\ V_1 &\sim -\frac{L_A^2 c_0^2 \zeta^2}{2} + L_A c_1 \zeta + \cdots, \\ W_1 &\sim \left(\frac{\overline{\beta}}{c_0^2}K_\nu - B_0\right) L_W c_0 \zeta + B_1 \cdots, \end{aligned} \tag{34}$$

as $\zeta \to \infty$. Eliminating the reaction terms from Equations (33a,b), integrating and applying the matching conditions (29, 34), we find

$$U_1' + c_0 U_0 - \left(\frac{1}{L_A}V_1' + c_0 V_0\right) = \frac{\overline{\alpha}}{\nu c_0}(1 - I_\nu), \quad W_1 = \left(\frac{\overline{\beta}}{c_0^2}K_\nu - B_0\right) L_W c_0 \zeta + B_1. \tag{35}$$

We now consider the region at the rear of the wave (Region III). In this region all the fuel has been used up, *i.e.* $v \equiv 1$. We find that this region consists of two subregions, Regions IIIa and IIIb. In Region IIIa we put

$$Y = \gamma^{-3/2}\, y, \qquad w = \gamma^{-1}\, \tilde{w} \tag{36}$$

and leave u unscaled. This results in the equations

$$\begin{aligned} u'' + \overline{c} u' - \frac{\overline{\alpha}}{\gamma}\left(1 - \frac{\tilde{w}}{\gamma}\right)\exp\left(\frac{\nu(u-1)}{u}\right) &= 0, \\ \frac{1}{L_W}\tilde{w}'' + \overline{c}\tilde{w}' + \overline{\beta}\left(1 - \frac{\tilde{w}}{\gamma}\right)\exp\left(\frac{\nu(u-1)}{u}\right) &= 0, \end{aligned} \tag{37}$$

where primes now denote differentiation with respect to Y.

We look for a solution of Equations (37) by expanding

$$u = u_0 + \gamma^{-1}u_1 + \cdots, \qquad \tilde{w} = \tilde{w}_0 + \gamma^{-1}\tilde{w}_1 + \cdots.$$

We find, on matching with the reaction zone (Region II)

$$u_0 = 1, \quad u_1 = \frac{\overline{\alpha}}{c_0}Y + T_1 + \frac{\overline{\alpha}I_\nu}{\nu c_0^2}, \quad \tilde{w}_0 = -\frac{\overline{\beta}Y}{c_0} + \left[\frac{\overline{\beta}}{c_0^2}(J_\nu - K_\nu) + B_0\right]. \tag{38}$$

Matching with Regions I and II then gives

$$B_0 = \frac{\overline{\beta}}{L_W c_0^2}(1 + K_\nu L_W)$$

To complete the solution we require Region IIIb, where we put

$$\xi = \gamma^{-5/2}\, y = \frac{Y}{\gamma} \tag{39}$$

and leave u and w unscaled. The leading order equations are

$$\begin{aligned} c_0\frac{\mathrm{d}u}{\mathrm{d}\xi} - \overline{\alpha}(1-w)\exp\left(\frac{\nu(u-1)}{u}\right) &= 0, \\ c_0\frac{\mathrm{d}w}{\mathrm{d}\xi} + \overline{\beta}(1-w)\exp\left(\frac{\nu(u-1)}{u}\right) &= 0, \end{aligned} \tag{40}$$

subject to, from (38),

$$u \sim 1 + \frac{\overline{\alpha}}{c_0}\xi + \cdots, \quad w \sim -\frac{\overline{\beta}}{c_0}\xi + \cdots \quad \text{as } \xi \to 0^-. \tag{41}$$

Adding equations (40), integrating and satisfying (41) we have

$$\overline{\beta}\,u + \overline{\alpha}\,w = \overline{\beta} \tag{42}$$

and then

$$c_0\frac{\mathrm{d}u}{\mathrm{d}\xi} = \left((\overline{\alpha} - \overline{\beta}) + \overline{\beta}u\right)\exp\left(\frac{\nu(u-1)}{u}\right), \quad \text{in } -\infty < \xi < 0, \quad u(0) = 1. \tag{43}$$

There are two cases to consider. If $\overline{\alpha} < \overline{\beta}$, Equation (43) has a steady state at $u = 1 - \overline{\alpha}/\overline{\beta}$ and this steady state is approached (from the given initial condition) as $\xi \to -\infty$. This gives the front wave. Note that $w \to 1$ as $\xi \to -\infty$ in this case, all the inhibitor is used up in the reaction. If $\overline{\alpha} > \overline{\beta}$, then the term on the right-hand side of Equation (42) is positive for all $1 > u > 0$ and here $u \to 0$ as $\xi \to -\infty$. This is a pulse wave, with $w \to \overline{\beta}/\overline{\alpha}$, consistent with (18) with $v_s = 1$.

We now return to the reaction zone (Region II). From (38)

$$U_1 \sim -\frac{\overline{\alpha}}{c_0}\zeta + \cdots, \quad V_1 \to 0 \quad \text{as } \zeta \to -\infty. \tag{44}$$

Applying (44) in (35a) we obtain

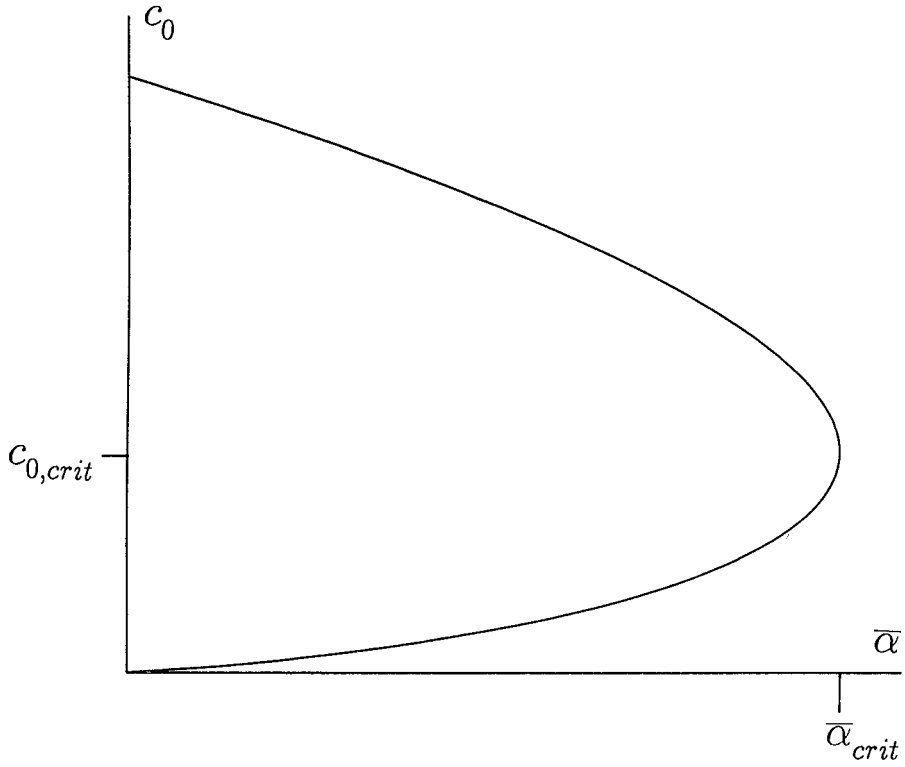

Figure 1. The solution to Equation (46) for c_0 in terms of $\overline{\alpha}$. $\overline{\alpha}_{\text{crit}}$ is given by (47).

$$T_1 = -\frac{\overline{\alpha}}{c_0^2}\left(\frac{\nu+1}{\nu}\right) \tag{45}$$

and hence, from (32),

$$c_0^2 = 4L_A^2 \exp\left(-\frac{\overline{\alpha}}{\nu c_0^2}(\nu+1-I_\nu)\right). \tag{46}$$

Equation (46) can be regarded as an equation for c_0 in terms of $\overline{\alpha}$. This equation has two solutions for c_0 for $0 < \overline{\alpha} < \overline{\alpha}_{\text{crit}}$ where

$$\overline{\alpha}_{\text{crit}} = 4L_A^2 e^{-1}\frac{\nu}{\nu+1-I_\nu}, \quad \alpha_{\text{crit}} \sim 4L_A^2 e^{-1}\frac{\nu}{\nu+1-I_\nu}\gamma^{-4} + \cdots \text{ as } \gamma \to \infty \tag{47}$$

with a corresponding $c_{0,\text{crit}} = 2L_A \mathrm{e}^{-1/2}$. There are no solutions for $\overline{\alpha} > \overline{\alpha}_{\text{crit}}$. A typical situation is illustrated in Figure 1. Note that expression (47) is independent of $\overline{\beta}$. In the present case ($\alpha \sim \beta \sim \gamma^{-4}$) there is extinction at a finite value of α (as given by (47)). There is the possibility of the transition from front waves (which always arise at $\alpha = 0$) to pulse waves provided $\overline{\beta} < \overline{\alpha}_{\text{crit}}$. Thus extinction, through the saddle-node bifurcation, can occur from both front and pulse solutions in this limit.

3.2. $\alpha \ll \beta$

We can modify the above analysis to the case when β is of $O(\gamma^{-3})$, still with α of $O(\gamma^{-4})$ and $\mu\gamma$ of $O(1)$. The main difference with the previous case is that w is now $O(1)$ in Regions I

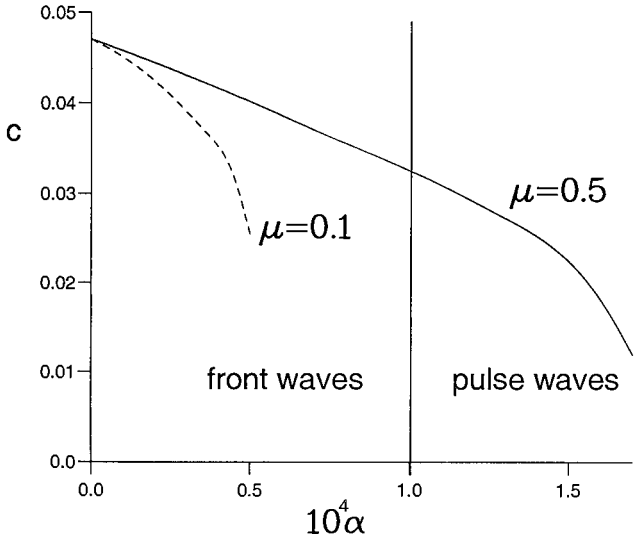

Figure 2. Wave speed c against α, obtained from the numerical integrations of initial-value problem (6–10), for $\gamma = 10{\cdot}0$, $\beta = 10^{-4}$ and $\mu = 0{\cdot}1, 0{\cdot}5$, ($L_A = L_W = 1$).

and II and that $w \equiv 1$ in Region III. In this case we get only front waves (as expected) and there is no wave extinction at a finite value of $\overline{\alpha}$, finding that

$$c_0^2 = 4L_A^2 \exp\left(-\overline{\alpha}/\tilde{\beta}\right), \tag{48}$$

where $\tilde{\beta} = \beta\gamma^3$ is $O(1)$.

We can extend the range of our analysis, still keeping the basic structure given above, to the case when α and β are $O(\gamma^{-2})$ and $O(\gamma^{-1})$, respectively, with μ now of $O(1)$. We write

$$\alpha = \hat{\alpha}\gamma^{-2}, \qquad \beta = \hat{\beta}\gamma^{-1},$$

where $\hat{\alpha}$, $\hat{\beta}$ are $O(1)$ as $\gamma \to \infty$. We still keep (19) as the scaling for the wave speed c and the scaling for y given in (21) for Region I, though now we take w to be $O(1)$ in this region. Allowing μ to be of $O(1)$ means that both reaction terms can be neglected in Region I. The terms u_0, v_0, v_1 in the expansion in γ^{-1} are the same as in (20), with now u_1 and w_0 taking the simpler forms, consistent with matching with the reaction zone,

$$u_1 = (T_1 - c_1\overline{y})\mathrm{e}^{-c_0\overline{y}}, \quad w_0 = \mathrm{e}^{-L_W c_0 \overline{y}}, \quad w_1 = -(c_1 L_W \overline{y} - B_1)\mathrm{e}^{-c_0 L_W \overline{y}}. \tag{49}$$

We still use scalings (24) for the reaction zone (Region II) though now we put

$$w = 1 - W\gamma^{-1}$$

This leads to the equations for the reaction zone as

$$\begin{aligned} U'' - V^2 \exp\left(-\frac{U}{1-\gamma^{-1}U}\right) + \gamma^{-1}\left[\overline{c}U' + \hat{\alpha}W\exp\left(-\frac{\mu U}{1-\gamma^{-1}U}\right)\right] &= 0, \\ \frac{1}{L_A}V'' - V^2\exp\left(-\frac{U}{1-\gamma^{-1}U}\right) + \gamma^{-1}\overline{c}V' &= 0, \\ \frac{1}{L_W}W'' + \gamma^{-1}\overline{c}W' - \hat{\beta}W\exp\left(-\frac{\mu U}{1-\gamma^{-1}U}\right) &= 0, \end{aligned} \tag{50}$$

subject to the matching conditions, found by expressing the solution in Region I for $\overline{y}$ small in terms of $\zeta = \gamma\overline{y}$, that

$$U \sim (c_0\zeta - T_1) + \gamma^{-1}\left(-\frac{c_0^2}{2}\zeta^2 + (c_1 + c_0T_1)\zeta + T_2\right) + \cdots,$$

$$V \sim L_Ac_0\zeta + \gamma^{-1}\left(-\frac{L_A^2c_0^2}{2}\zeta^2 + L_Ac_1\zeta\right) + \cdots, \tag{51}$$

$$W \sim (L_Wc_0\zeta - B_1) + \gamma^{-1}\left(-\frac{L_W^2c_0^2}{2}\zeta^2 + L_W(c_1 + c_0B_1)\zeta + B_2\right) + \cdots,$$

as $\zeta \to \infty$. We look for a solution to Equations (50) by expanding in γ^{-1}. At leading order we obtain Equations (28a,b), from which it follows (as before), on integrating and applying matching conditions (51), that

$$U_0 = \frac{1}{L_A}V_0 - T_1, \quad U_0'^2 = c_0^2 - 2L_A^2\mathrm{e}^{-U_0}\left((U_0 + T_1)^2 + 2(U_0 + T_1) + 2\right). \tag{52}$$

Since $V_0 \to 0$ at the rear of the reaction zone

$$U_0 \to -T_1 \text{ as } \zeta \to -\infty, \quad \text{and } c_0^2 = 4L_A^2\mathrm{e}^{T_1}. \tag{53}$$

From Equation (50c)

$$W_0'' - \hat{\beta}W_0\mathrm{e}^{-\mu U_0} = 0, \quad W_0 \sim c_0L_W\zeta - B_1 \text{ as } \zeta \to \infty. \tag{54}$$

At $O(\gamma^{-1})$ we obtain, on eliminating the reaction terms (using (53)), integrating and applying the matching conditions as $\zeta \to \infty$,

$$U_1' + c_0U_0 - \left(\frac{1}{L_A}V_1' + c_0V_0\right) + \frac{\hat{\alpha}W_0'}{\hat{\beta}L_W} = \frac{\hat{\alpha}c_0}{\hat{\beta}}. \tag{55}$$

In this case Region III is redundant as the reaction terms can be neglected in this region (with μ of $O(1)$ and γ large) with then u a constant $\sim 1 + T_1\gamma^{-1} + \cdots$, $v \equiv 1$, $w \equiv 1$. Hence, $U_1' \to 0$, $V_0 \to 0$, $W_0 \to 0$ as $\zeta \to -\infty$ so that (54) gives

$$U_0 \to \frac{\hat{\alpha}}{\hat{\beta}} = -T_1 \quad \text{as } \zeta \to -\infty. \tag{56}$$

Then, from (53) and (56) we obtain

$$c_0^2 = 4L_A^2\mathrm{e}^{-\hat{\alpha}/\hat{\beta}}, \qquad c \sim \frac{2L_A\mathrm{e}^{-\alpha\gamma/2\beta}}{\gamma^{3/2}} + \cdots \text{ for } \gamma \gg 1,\ \alpha\gamma \sim \beta. \tag{57}$$

The above analysis shows that there is an interplay between α (the heat lost in the endothermic reaction (2)) and β (the rate at which the inhibitor is consumed) for the formation of combustion waves. It suggests that we require α to be small. With $\beta \sim \alpha$ there is extinction at a finite rate of heat loss, α_{crit} (expression (47)), and the possible change from fronts (all the fuel and inhibitor consumed) to pulses (temperature returns to its original value, some fuel and inhibitor remaining). With $\beta \gg \alpha$ there is a rapid (exponential) fall off in wave speed with α (for given values of the other parameters), see expression (57). There is also the suggestion from this analysis that wave formation will be inhibited if α is sufficiently large

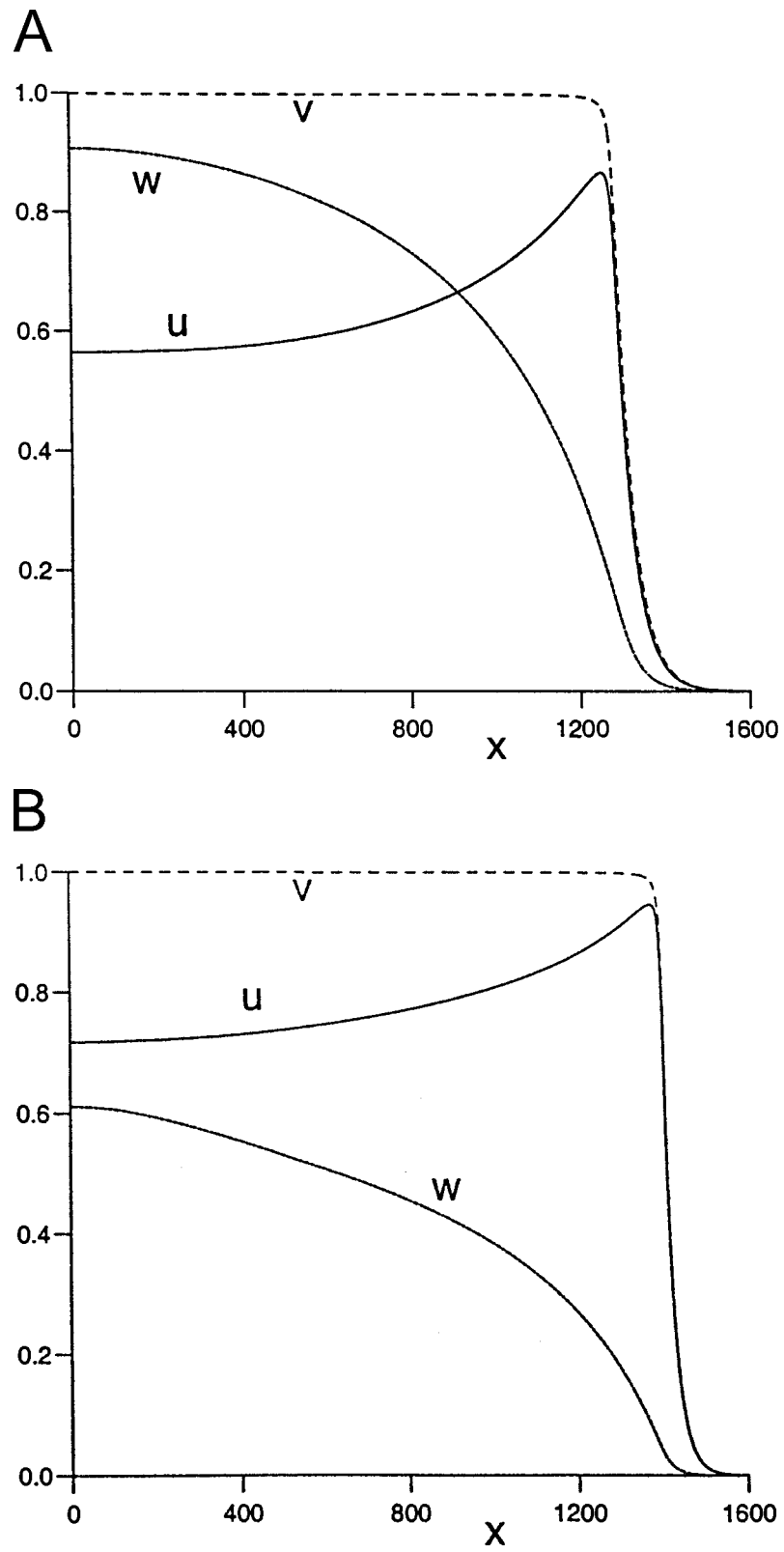

Figure 3. Wave profiles for $\gamma = 10{\cdot}0$, $\beta = 10^{-4}$ ($L_A = L_W = 1$) and (a) $\mu = 0{\cdot}.1, \alpha = 5 \times 10^{-5}$, (b) $\mu = 0{\cdot}5$, $\alpha = 5 \times 10^{-5}$, (c) $\mu = 0{\cdot}5, \alpha = 1{\cdot}7 \times 10^{-4}$. — u, – – – v, - - - - w.

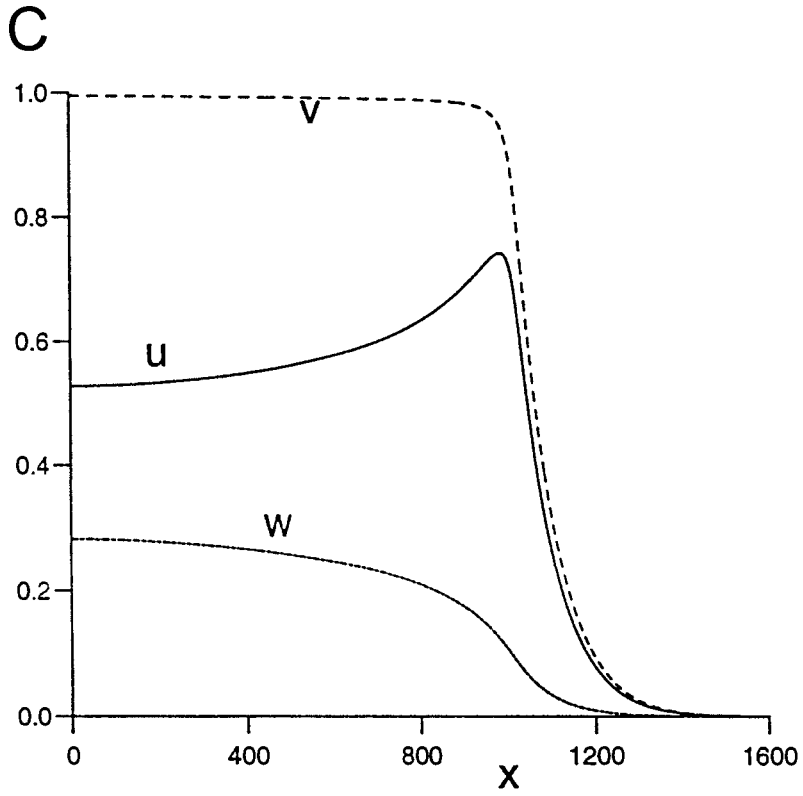

Figure 3. Continued.

(unless we formally put $\beta \equiv 0$). We now test these predictions from our high-activation-energy asymptotics through numerical integrations of the original initial-value problem (6–10).

4. Numerical simulations

Equations (6–8), subject to initial and boundary conditions (9,10), were solved numerically using a standard scheme for integrating parabolic systems based on the Crank-Nicolson method. The sets of nonlinear finite-difference equations that arise in the method are solved in turn using Newton-Raphson iteration. A space step $\Delta x = 0{\cdot}1$ was used for the results shown, with the number of grid points varying from 8,000 to 16,000 as required by the nature of the combustion waves that form. A variable time step Δt was used. This was adjusted to keep the errors introduced in time differencing within some preset tolerance by covering the step from t to $t + \Delta t$ in one and then two steps and requiring that the difference between these two solutions was less than this tolerance (usually set to 5×10^{-4}). The more acurate (two-step solution) was used to start the integration for the next time step. A routine was incorporated into the numerical integrator to monitor the position of the wave, located at the point where the fuel concentration achieved half its maximum possible value. The variation of this with t was calculated to give the wave speed c.

Some initial trial runs were performed with a smaller space step of $\Delta x = 0{\cdot}05$. These were compared with the corresponding runs with $\Delta x = 0.1$ and relatively small differences (well

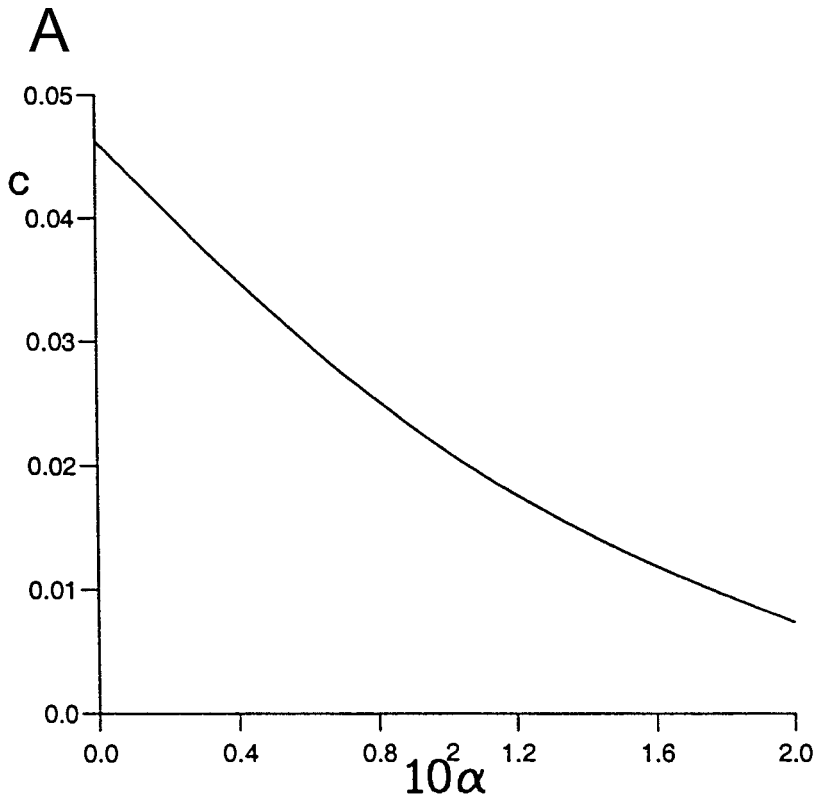

Figure 4. (a) wave speed c against α, obtained from the numerical integrations of initial-value problem (6–10), for $\gamma = 10{\cdot}0$, $\beta = 0{\cdot}1$ and $\mu = 0{\cdot}5$ ($L_A = L_W = 1$). (b) wave profiles for $\gamma = 10{\cdot}0$, $\beta = 0{\cdot}1$, $\mu = 0{\cdot}5$ and $\alpha = 0{\cdot}0175$. — u, – – – v, - - - - w.

within graphical accuracy) were found between the two sets of results. This gave us confidence that using $\Delta x = 0{\cdot}1$ would give reliable accuracy. Our analysis shows that a reaction region develops that is relatively thin (with large gradients), at least for the larger values of γ, and the number of grid points within this region needs to be sufficiently large to maintain accuracy. We monitored this point and found that taking $\Delta x = 0{\cdot}1$ gave over 1200 grid points within the reaction region in the extreme cases, often there were many more than this. We thought that this was satisfactory for the accuracy required. To deal with applying the unburnt gas temperature $T = 0$ ahead of the wave, in the numerical scheme we set the reaction terms to zero if the temperature was below some small positive value, taken as the tolerance for the convergence of the Newton-Raphson iteration.

We start by considering a case typical of $\alpha \sim \beta \sim \gamma^{-4}$, taking $\gamma = 10{\cdot}0$ and $\beta = 10^{-4}$. Plots of the wave speed c against α, calculated from the numerical integrations for $\mu = 0{\cdot}1$ and $\mu = 0{\cdot}5$, are shown in Figure 2. We took $L_A = L_W = 1$ as we do in the rest of the numerical solutions described below. The graph shows that the wave speed decreases with μ (for a given α) with wave extinction at a finite value of α, α_{crit}, in both cases. For $\mu = 0{\cdot}5$ there is a transition from front to pulse waves before this extinction. (The position of the transition from fronts to pulses is marked on Figure 2.) This is not the case for $\mu = 0{\cdot}1$ where only front waves form. The numerical integrations give $\alpha_{\text{crit}} = 6{\cdot}7 \times 10^{-5}$ for $\mu = 0{\cdot}1$ and $\alpha_{\text{crit}} = 1{\cdot}7 \times 10^{-4}$ for $\mu = 0{\cdot}5$. Expression (47) suggests corresponding values of $\alpha_{\text{crit}} = 9{\cdot}8 \times 10^{-5}$ and $1{\cdot}19 \times 10^{-4}$.

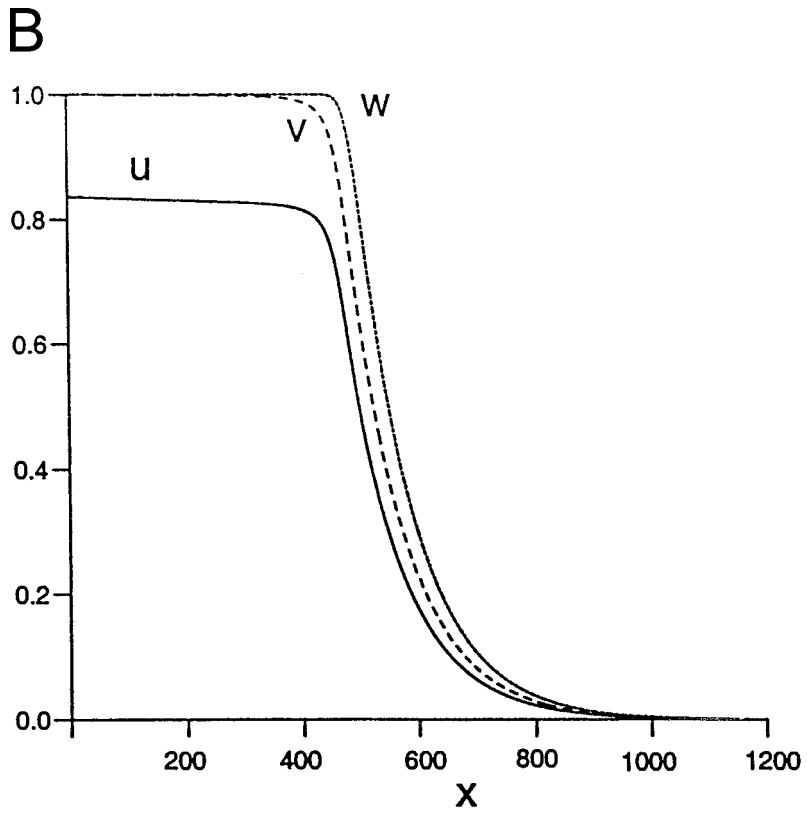

Figure 4. Continued.

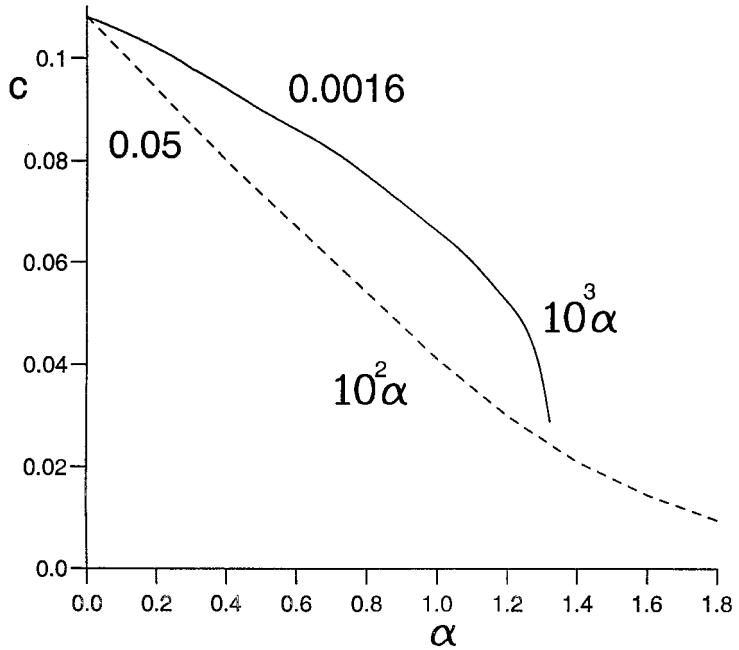

Figure 5. Wave speed c against α, obtained from the numerical integrations of initial-value problem (6–10), for $\gamma = 5{\cdot}0$, $\mu = 0{\cdot}5$ and $\beta = 0{\cdot}05, 0{\cdot}0016$ ($L_A = L_W = 1$).

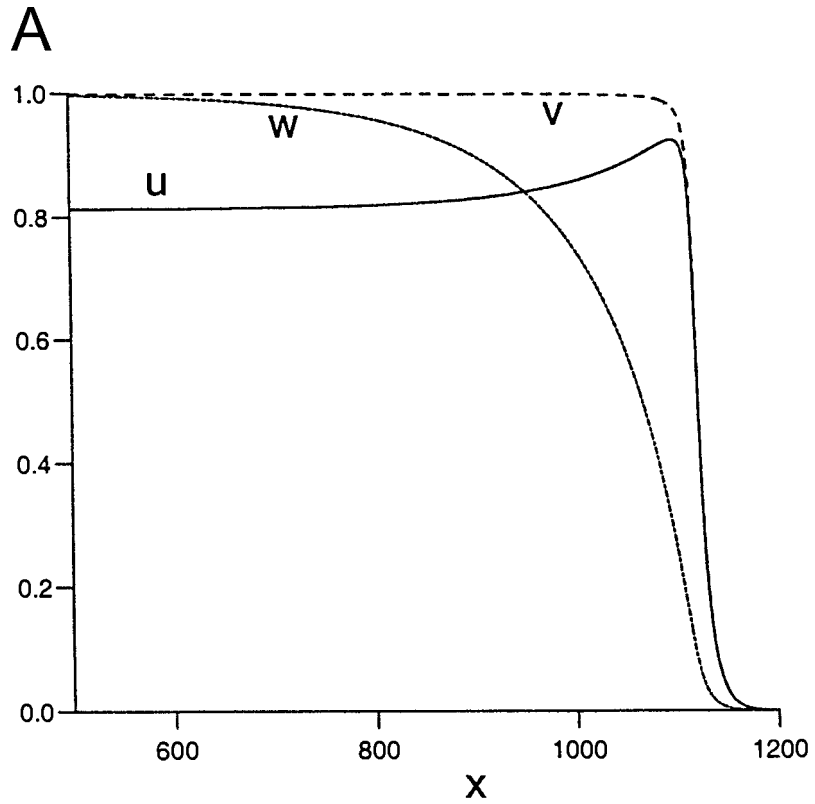

Figure 6. Wave profiles for $\gamma = 5{\cdot}0$, $\mu = 0{\cdot}5$ ($L_A = L_W = 1$) and (a) $\alpha = 3 \times 10^{-4}$, $\beta = 0{\cdot}0016$, (b) $\alpha = 0{\cdot}006$, $\beta = 0{\cdot}05$, (c) $\alpha = 0{\cdot}016$, $\beta = 0{\cdot}05$. — u, – – – v, - - - - w.

Reasons for this difference could lie in that the value of γ needs to be larger for the leading order terms in our asymptotic analysis to be a more accurate representation. Errors could also arise from μ not being sufficently small. These differences between theory and numerics can be seen in the wave speeds. For example, c_{ad}, the adiabatic wave speed ($\alpha = 0$) is, from (46), $c_{\mathrm{ad}} \sim 2L_A\gamma^{-3/2} = 0{\cdot}063$ in the present case, whereas we find $c_{\mathrm{ad}} = 0{\cdot}047$ in the numerical integrations.

Figure 3 shows wave profiles for this case ($\gamma = 10$, $\beta = 10^{-4}$) plotted on a long spatial domain well after initiation. Figures 3a,b illustrate the development of front waves for $\alpha = 5 \times 10^{-5}$ and $\mu = 0{\cdot}1$ (Figure 3a) and $\mu = 0{\cdot}5$ (Figure 3b). These figures show behaviour in the reaction zone in line with theory, with the u and v profiles almost identical (expression (30)) and with only a small increase in the concentration of w (see scaling (24)). The v concentration rapidly approaches its totaly consumed value of $v = 1$ at the rear of the reaction zone, though u and w have not fully recovered to their final values in this plot (Region III of the theory) of $u \to 1 - \alpha/\beta = 0{\cdot}5$, $w \to 1$. This effect is more noticable with $\mu = 0{\cdot}5$ than for $\mu = 0{\cdot}1$. We could expect this from theory, since the final recovery region (Region IIIb) is large, having an extent of $O(\gamma^{5/2})$. In both cases temperatures higher than the final outcome are achieved within the reaction zone, again in line with scaling (24) which gives $u = 1 + O(\gamma^{-1})$ in the reaction zone.

Figure 2 shows that only front waves can form when $\mu = 0{\cdot}1$. However, pulse waves are possible for $\mu = 0{\cdot}5$. We illustrate the development of a pulse wave in Figure 3c (for $\alpha =$

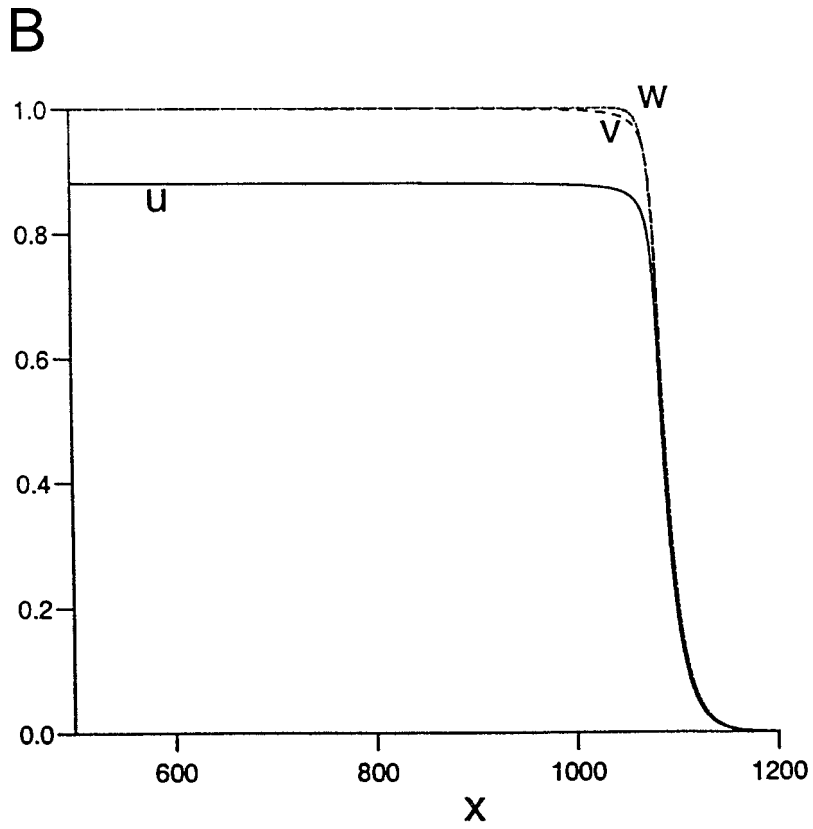

Figure 6. Continued.

$1{\cdot}7 \times 10^{-4}$). The speed of this wave is reduced from that seen in Figure 3b (from $c = 0{\cdot}040$ to $c = 0{\cdot}011$). The behaviour in the reaction zone is similar in both cases with v again rapidly achieving its final value. Now the final states for u and w ($u \to 0$, $w \to \beta/\alpha = 0{\cdot}588$) are a long way from being reached. We can gain some insight into the reason why this is the case from Equation (43), which becomes

$$c_0 \frac{\mathrm{d}u}{\mathrm{d}\xi} = (\bar{\alpha} - \bar{\beta})\mathrm{e}^{-\frac{v}{u}} \qquad \text{for } u \text{ small.} \tag{58}$$

Equation (58) shows that the approach over this region of extent $O(\gamma^{5/2})$ to $u = 0$ is extremely slow, with

$$u \sim \frac{v}{\log\left[\dfrac{c_0 v|\xi|(\log|\xi|)^2}{(\bar{\alpha} - \bar{\beta})}\right]} + \cdots \qquad \text{as } \xi \to -\infty.$$

The behaviour of w follows from (42) as

$$w \sim \frac{\bar{\beta}}{\bar{\alpha}}\left(1 - \frac{v}{\log\left[\dfrac{c_0 v|\xi|(\log|\xi|)^2}{(\bar{\alpha} - \bar{\beta})}\right]} + \cdots\right) \qquad \text{as } \xi \to -\infty.$$

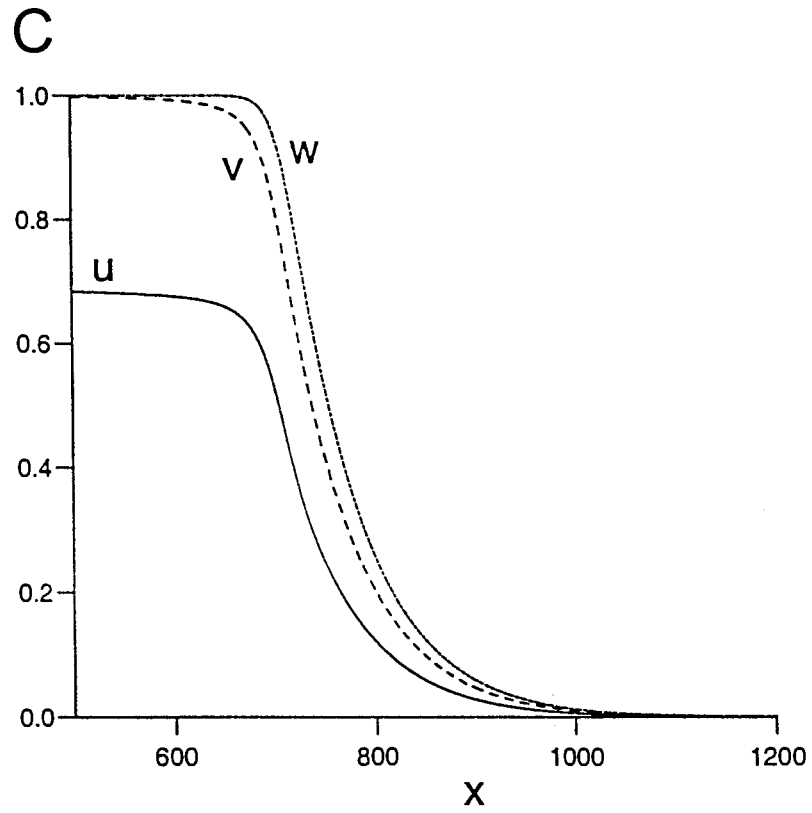

Figure 6. Continued.

This very slow decay to final asymptotic conditions could be expected, since in this final region the reaction has almost switched off, being no more than of $O(e^{-\gamma})$ for γ large, and the profiles are very flat, so diffusion and thermal conduction also have little effect in reducing u to zero (and increasing w to its final value).

Our theory predicted different behaviour when β is $O(\gamma^{-1})$, much larger than the previous case. We illustrate this case in Figure 4a with a plot of the wave speed c against α for $\gamma = 10{\cdot}0$ and $\mu = 0{\cdot}5$. Here there is no extinction at a finite value of α, though the wave speed becomes very small for the higher values of α (with α still small compared to β). The slope of the curve is similar to that suggested by expression (57), though, as before, the theoretically predicted values are somewhat larger than those determined numerically. The main point to note is that there is a qualitative difference between this case (Figure 4a) and the previous case (Figure 2). We show wave profiles in Figure 4b (for $\alpha = 0{\cdot}0175$). The figure shows that there is a separation between the three profiles, with the inhibitor being consumed ahead of the fuel in the preheat zone (Region I), with the temperature then rising in the reaction zone as a result of fuel consumption. Here the u profile is monotone, u achieves its maximum value after the reaction (compare with Figure 3). In this case only front waves can form and both v and w reach their final values rapidly at the end of the reaction zone though u takes longer to settle to its final value ($u \to 0{\cdot}825$).

The behaviour identified theoretically for γ large and seen in the numerical simulations for $\gamma = 10$ holds for smaller values of γ. This is shown in Figure 5, where we plot the wave speed c against α for $\gamma = 5{\cdot}0$ (with $\beta = 0{\cdot}0016$ and $\beta = 0{\cdot}05$). (Note the the different scales

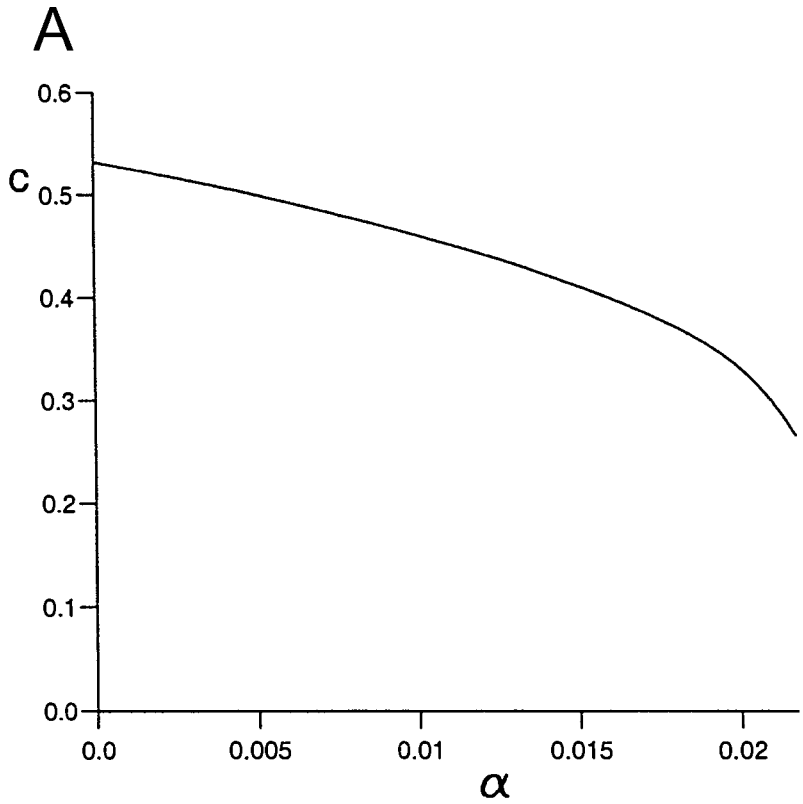

Figure 7. (a) wave speed c against α, obtained from the numerical integrations of initial-value problem (6–10), for $\gamma = 1{\cdot}0$, $\beta = 0{\cdot}005$ and $\mu = 0{\cdot}5$ ($L_A = L_W = 1$). Wave profiles for $\gamma = 1{\cdot}0$, $\beta = 0{\cdot}005$, $\mu = 0{\cdot}5$ and (b) $\alpha = 0{\cdot}003$, (c) $\alpha = 0{\cdot}02$. — u, – – – v, - - - - w.

for α used in this plot.) In the former case $\beta \sim \gamma^{-4}$ and behaviour suggested by expression (46) is seen (see Figure 2) with extinction at $\alpha_{\text{crit}} = 0{\cdot}00133$. In the latter case $\beta \sim \gamma^{-1}$ and behaviour identified by expression (57) results (see Figure 4a). Note that for the results shown in the figure the ratio $\alpha\gamma/\beta$ is of $O(1)$.

Typical wave profiles (front waves) for these two cases are shown in Figure 6. Figure 6a ($\beta = 0{\cdot}0016$, $\alpha = 3 \times 10^{-3}$) shows profiles similar to those seen in Figure 3a, though now the final conditions ($u \to 0{\cdot}8125$, $v, w \to 1$) are achieved more readily after the reaction zone has passed. There is still an 'overshoot' in the temperature within the reaction zone. Note that the influence of the initiation can be seen in a region near the origin where a temperature excess still remains. This feature is also seen in Figures 6b,c. For Figures 6b,c we took $\beta = 0{\cdot}05$, with a small value of α for Figure 6b ($\alpha = 0{\cdot}016$). For small α the wave profiles are almost indentical in the reaction zone, different to the behaviour mentioned previously (Figure 4b). For higher values of α (Figure 6c) the wave profiles become more separated (as in figure 4b). An important difference between the the profiles shown in Figures 6a and 6c is that, in the former case (smaller β), the reaction in the fuel starts first before the reaction in the inhibitor, nearly all the fuel has been consumed before there is any appreciable loss of inhibitor. This is not the case for higher β (Figure 6c) where the reaction in the inhibitor starts first.

Extinction at a finite value of the cooling parameter α is not restricted to having a high activation energy (large γ). This can be seen in Figure 7a, where we plot wave speeds c

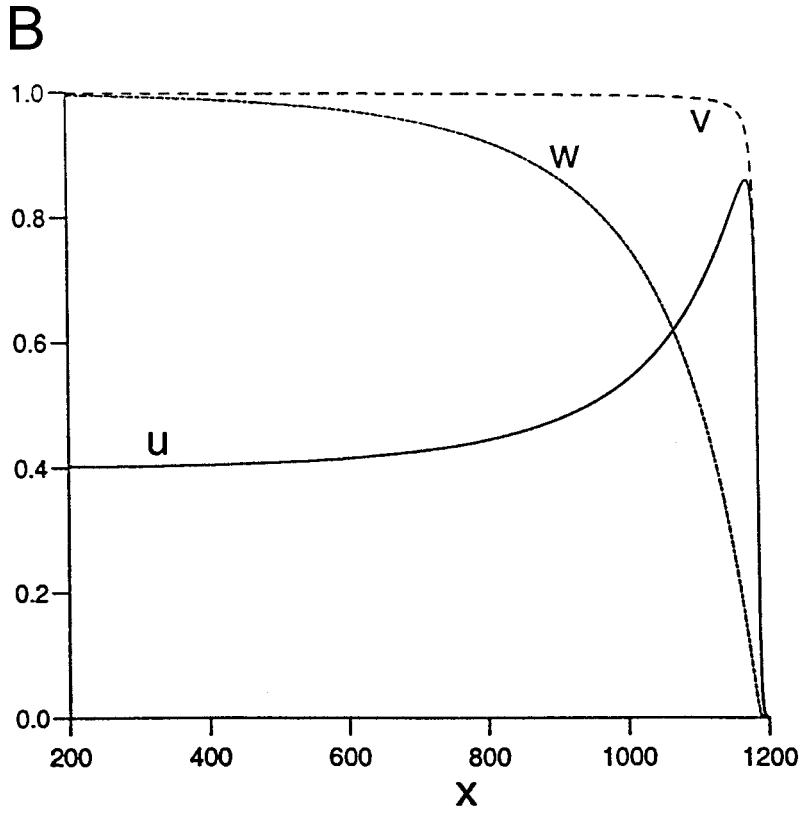

Figure 7. Continued.

against α for $\gamma = 1{\cdot}0$ (and $\beta = 0{\cdot}005$, $\mu = 0{\cdot}5$). In this case $\alpha_{\text{crit}} = 0{\cdot}0217$, showing, with the previous results, that the range of α over which wave initiation is possible increases as γ is decreased. For smaller values of γ we may expect the final state of the system to be achieved more readily after the wave has passed. This is the case for front waves, as can be seen in Figure 7b (here $\alpha = 0{\cdot}003$). Pulse waves in the temperature take much longer to form even at this low value of γ, as can be seen in Figure 7c (for $\alpha = 0{\cdot}02$). This figure shows that there is still a drop to be achieved in the u profile before the pulse is fully formed, though the pulse-like structure of this wave is much clearer than that shown in Figure 3c.

5. Discussion

We have identified two different types of behaviour that can be supported by our combustion model. Which type occurs depends most strongly on the parameters α and β, the other parameters μ and γ are not especially significant in determining the qualitative behaviour. We can think of α as a heat-loss parameter — it represents the heat lost in the endothermic decay of the inhibitor relative to that produced by the exothermic combustion of the fuel. The parameter β represents the rate at which inhibitor is consumed relative to the consumption of fuel. With β small this is a weak process. Even so, the heat lost through this endothermic reaction has a strong quenching effect on wave initiation, combustion waves forming only when $\alpha < \alpha_{\text{crit}}$ with $\alpha_{\text{crit}} \sim \beta$. This effect is analogous to the extinction of wave propagation when heat is lost through Newtonian coooling [4–6], where usually only weak cooling rates are needed

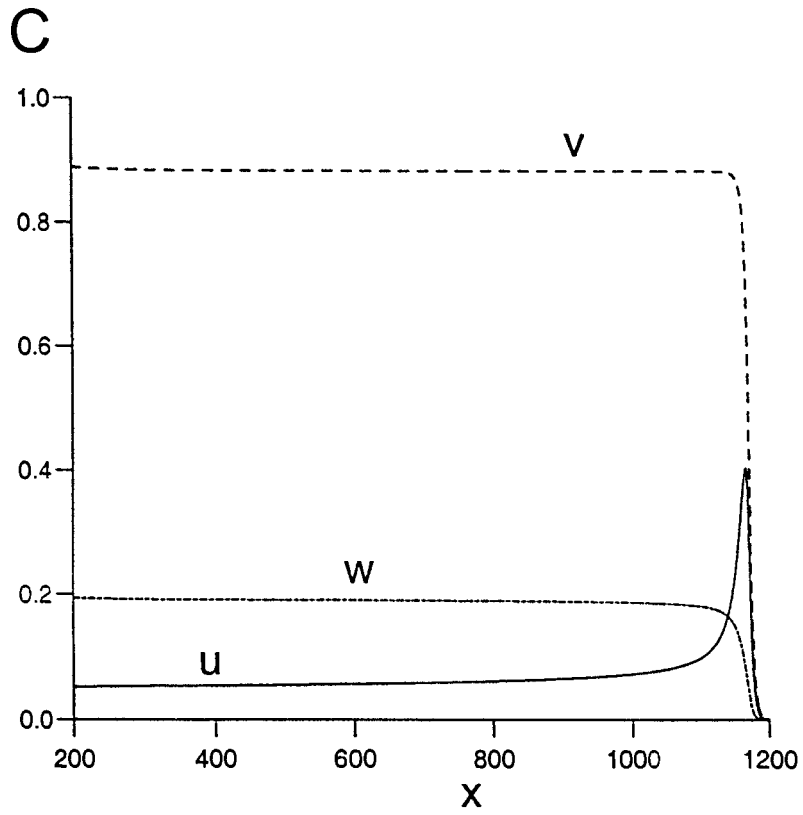

Figure 7. Continued.

to induce extinction. The wave speed — cooling parameter curves are similar in both cases (Figures 2, 5 and 7a). In analogy we can expect a saddle-node bifurcation in our case at α_{crit} (see Figure 1) with the lower branch being unstable (and hence unattainable in our numerical simulations).

For larger values of β and stronger inhibitor decay rates, the effect of the endothermic cooling is to quickly reduce the wave speed as the cooling parameter α is increased (Figures 4a and 5). For propagating waves to form in this case requires $\alpha \ll \beta$. There are distinct differences in the combustion waves that form in the two cases (Figures 3, 4b, 6a,c) reflecting the significance of inhibitor decay relative to fuel consumption.

Some confirmation of the qualitative different behaviour supported by our model is provided by studies (both experimental and theoretical) on the inhibitory effects that the addition of sprays or particles (both reactive or inert) can have on premixed flame propagation [11–18]. These studies have shown that the propagation speed of a premixed flame is decreased by the addition of dust (or spray) through negative thermal (and sometimes chemical) feedback. The main parameters on which the flame speed depended were found to be the virtual heat capacity of the particles and the particle size. The speed was found to decrease either monotonically (as in our $\alpha\gamma \sim \beta \sim \gamma^{-1}$ case) or to have an *S*–shaped form (depending on the value of the particle–size parameter). The upper branch of this latter curve is similar to our $\alpha \sim \beta \sim \gamma^{-4}$ case.

A feature of our results is the large difference between the theoretically and numerically determined values, even at the largest value of γ considered ($\gamma = 10$). This appears to

be a general feature of high-activation-energy asymptotics. The differences between theory and numerics seen in our model are comparable with those seen when there is heat loss by Newtonian cooling, where much higher activation energies are needed to get much better agreement. So it is, perhaps, not surprising that we see such differences in the two sets of results, though we can still have confidence that the behaviour found in our high-activation asymptotics is a reliable guide to how the system behaves in general.

Acknowledgements

AL wishes to thank ORS and the University of Leeds for financial support.

References

1. J.D. Buckmaster and G.S.S. Ludford, Theory of laminar flames. Cambridge: Cambridge University Press (1982) 266 pp.
2. F.A. Williams, Combustion theory. New York: Benjamin (1985) 680 pp.
3. Ya.B. Zeldovich, G.I. Barenblatt, V.B. Librovich and G.M. Makhviladze, The mathematical theory of combustion and explosion. Consultants Bureau (1985) 597 pp.
4. J. Buckmaster, The quenching of deflagration waves. *Combustion and Flame* 26 (1976) 151–162.
5. L. Galngetas and J.M. Roquejoffre, Bifurcation of travelling waves in a flame propagation model. *Cr. Acad. Sci. Paris* 31 (1994) 389–393.
6. B.H. Chao and C.K. Law, Laminar flame propagation with volumetric heat loss and chain branching termination reactions. *Int. J. Heat Mass Transfer* 37 (1994) 637–680.
7. B.F. Gray, S. Kalliadasis, A. Lazarovici, C. Macaskill, J.H. Merkin and S.K. Scott, The suppression of an exothermic branched– chain flame through endothermic reaction and radical scavenging. in Proc. Soc. Lond. Accepted for publication.
8. R.O. Weber, G.N. Mercer, H.S. Sidhu and B.F. Gray, Combustion waves for gases ($Le = 1$) and solids ($Le \to \infty$). *Proc. R. Soc. London* A453 (1997) 1105–1118.
9. G.N. Mercer, R.O. Weber and H.S. Sidhu, An oscillatory route to extinction for solid fuel combustion waves due to heat losses. *Proc. R. Soc. London* A454 (1998) 2015–2022.
10. H. Jeffreys and B.S. Jeffreys. *Methods of Mathematical Physics*. Cambridge: Cambridge University Press (1962) 716 pp.
11. J.B. Greenberg, A.C. McIntosh and J. Brindley, Linear stability analysis of laminar premixed spray flames. *Proc. R. Soc. London* A457 (2001) 1–31.
12. T. Mitani, A flame inhibition theory by inert dust and spray. *Combust. Flame* 43 (1981) 243–253.
13. A.M. Lentati and H.K. Chelliah, Dynamics of water droplets in a counterflow field and their effect on flame extinction. *Combust. Flame* 115 (1998) 158–179.
14. C.C. Liu, T.H. Lin and J.H. Tien, Extinction theory of stretched premixed flames by inert sprays. *Combust. Sci. Technol.* 91 (1993) 309–327.
15. G.O. Thomas, On the conditions required for explosion mitigation by water sprays. *Process Safety and Environment* 78 (2000) 339–354.
16. T. Mitani, A study on thermal and chemical effects of heterogeneous flame suppressants. *Combust. Flame* 44 (1982) 247–260.
17. T. Mitani, Flame retardant effects of CF_3Br and $NaHCO_3$. *Combust. Flame* 50 (1983) 177–188.
18. T. Mitani and T. Niioka, Extinction phenomena of premixed flames with alkali metal compounds. *Combust. Flame* 55 (1984) 13–21.